Met. Mater. Int., Vol. 21, No. 6 (2015), pp. 991~999
doi: 10.1007/s12540-015-5252-6

Adiabatic Shear Banding and Cracking Phenomena Occurring During Cold-Forging Simulation Tests of Plain Carbon Steel Wire Rods by Using a Split Hopkinson's Pressure Bar

Minju Kang[1], Jaeyeong Park[1], Seok Su Sohn[1], Hyunmin Kim[2], Kwan-Ho Kim[3], and Sunghak Lee[1]

[1]Center for Advanced Aerospace Materials, Pohang University of Science and Technology, Pohang 790-784, Korea
[2] School of Engineering, Brown University, Providence, RI 02912, USA
[3]Technical Research Laboratories, POSCO, 1 Goedong-dong Nam-gu, Pohang, Gyeongbuk 790-785, Korea

(received date: 18 May 2015 / accepted date: 6 July 2015)

Adiabatic shear banding and cracking phenomena occurring during cold forging of plain carbon steel wire rods, whose carbon content was varied from 0.2 to 0.8 wt%, were analyzed by forging simulation test using a split Hopkinson's pressure bar. The test results indicated that the 0.2C and 0.3C steels were dynamically compressed without surface defects after the fifth hit, whereas a deep crack was formed along the 45° direction in the 0.8C steel. In all the steels, adiabatic shear bands were formed diagonally inside forging-simulated specimens, and grains were extremely elongated within shear bands. The higher the volume fraction of pearlite was, the easier was the adiabatic shear banding. Particularly in the 0.8C steel, the shear band was white-colored and narrow, along which a long crack was formed. After the spheroidization treatment of the 0.8C steel, adiabatic shear bands or cracks were not found during the forging simulation test as the steel was relatively homogeneously deformed, which indicated that the spheroidization effectively prevented the adiabatic shear banding or cracking. The present forging simulation test plausibly evaluated the cold-forging performance by controlling the number and amount of hit, and provided an important idea on whether the spheroidization was needed or not.

Keywords: forging, adiabatic shear banding, strain rate, split Hopkinson's pressure bar, impact test

1. INTRODUCTION

Cold-heading-quality steel wire rods are mainly used for connecting parts such as bolts, nuts, and threads in many industrial areas including automobiles, machineries, electronics, and constructions. These rods are mostly classified into heat-treated and non-heat-treated ones, and are fabricated by various processes of drawing, forging, and heat-treatment. Heat-treated rods are generally spheroidized before cold drawing or forging processes. Recently developed non-heat-treated rods are subjected to cold drawing or forging to achieve required mechanical properties without spheroidization, which can give economical merits of fabrication costs and productivity [1-4]. However, these non-heat-treated rods often show low toughness in final products or induce the crack formation during high-strain-rate deformation processes such as cold forging.

In cold forging, materials with high formability which can accommodate severe deformation are required; plain carbon steels are widely used for these materials. However, cracks often form at the edges of components where deformation is highly concentrated. These cracks are generally associated with the formation of adiabatic shear bands, and their rapid propagation results in defective parts [5-8]. Local concentration of plastic deformation may arise under dynamic loading, and this plastically localized region is called an adiabatic shear band. This shear band, developed by thermo-mechanical instability, is reported to occur in titanium, aluminum, and copper alloys as well as in steels [6,9-15]. When shear bands are formed, load carrying capability of the regions is radically deteriorated, thereby causing the crack formation [8,16,17]. For example, the formation of shear bands occurring during cold forging induces the cracking. Thus, studies on the formation of shear bands are essential in improving microstructure and dynamic properties, controlling high-speed forming process, and preventing cracking. However, systematic studies have yet to be made to explain the cracking phenomenon in relation with microstructural parameters and their effect on formability. Furthermore, very few studies on how to solve this cracking problem frequently occurring during cold forging have been conducted. For the successful

*Corresponding author: shlee@postech.ac.kr

prevention of the cracking, the dynamic compressive deformation behavior, which can be closely related with the cold-forging process, should be verified. From these understandings, it is possible to successfully fabricate final products from cold-heading-quality steel wire rods without any defects or cracks.

In the present study, ferrite-pearlite microstructures of plain carbon steels were fabricated by varying C content, and their cracking possibilities were evaluated by a cold-forging simulation test using a split Hopkinson's pressure bar. Formation of the adiabatic shear band was investigated by examining deformed microstructures of the forging-simulated specimens, and the correlation of microstructures and dynamic compressive properties was clarified. Effects of microstructural evolution on dynamic deformation were also investigated so as to suggest the proper forging process and to prevent the cracking.

2. EXPERIMENTAL PROCEDURE

2.1. Plain carbon steel wire rods

Chemical compositions of four wire rods of plain carbon steels are shown in Table 1. The steels containing 0.22C, 0.35C, 0.45C, and 0.82C (wt%) are referred to as '2C', '3C', '4C', and '8C', respectively, because they have different C contents. The 2C, 3C, and 4C steels consist of ferrite and pearlite, whereas the 8C steel has a full pearlitic microstructure. A bloom of 300×400×6400 mm in size made by continuous casting was homogenized at 1250 °C for 5 hours at a furnace, and was rolled to make billets of 160×160 mm in cross-sectional area. The billets were held at 1200 °C for 3 hours, and were rolled again to make wire rods of 13 to 16 mm in diameter.

Table 1. Chemical compositions of the four plain carbon steel wire rods (wt%)

Steel	C	Mn	Si	P+S	Cr
2C	0.22	0.7	0.1 to 0.2	< 0.04	-
3C	0.38				-
4C	0.45				-
8C	0.82				0.2

2.2. Microstructural analysis

The fabricated wire rods were cross-sectioned in parallel to the rolling direction, polished, and etched in a nital solution. The center region was observed by an optical microscope and a scanning electron microscope (SEM, model; JSM-6330F, JEOL, Japan), and the volume fraction of pearlite was measured by an image analyzer. Hardness in the center region was measured by a Vickers hardness tester under 300 g load.

2.3. Dynamic compressive test

A split Hopkinson's pressure bar was used for dynamic compressive tests [18,19], whose schematic diagram is presented in Fig. 1. Cylindrical specimen (diameter; 5 mm, height; 5 mm) used for the dynamic compressive test was prepared in parallel to the rolling direction. The specimen was situated between incident and transmission bars, and was compressed by a striker bar (diameter; 19 mm) projected at a high speed using an air pressure of 0.2 MPa (impact velocity; 26.7 m/s). The compressive strain rate could be controlled by varying the pressure, and the strain rate obtained from the pressure of 0.1 MPa was about 2000/s. During the dynamic compression, the incident wave, reflective wave, and transmitted wave were respectively detected at strain gages, and recorded at an oscilloscope. Among the recorded wave signals, average compressive strain rate expressed as a function of time was measured from the reflected wave, while compressive stress expressed as a function of time was measured from the transmitted wave. Dynamic compressive stress-strain curves were obtained from these two parameters by eliminating the time term. Detailed descriptions of the dynamic test are provided in references [18,19].

2.4. Cold-forging simulation test

Figure 2 shows fabrication processes of an actual compo-

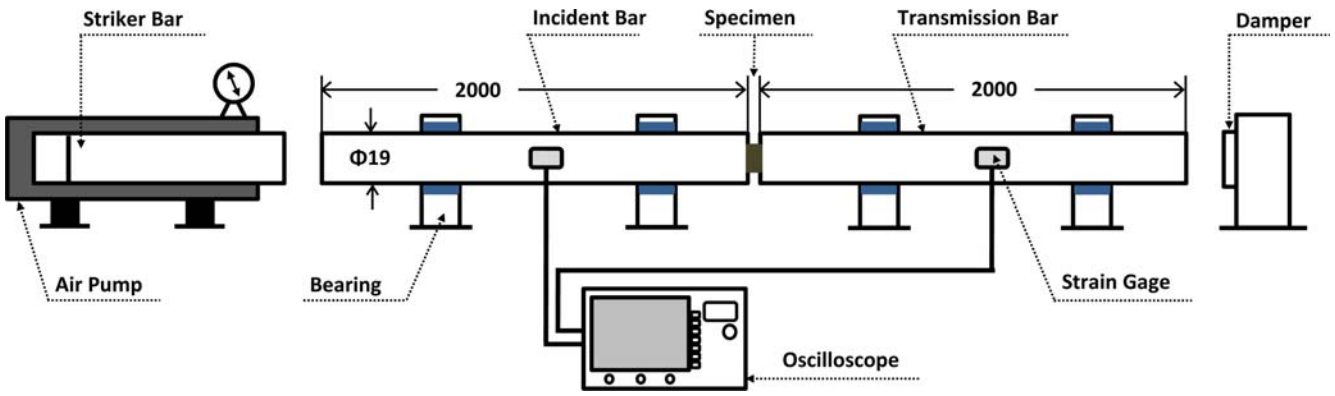

Fig. 1. Schematic diagram of the split Hopkinson's pressure bar (unit: mm).

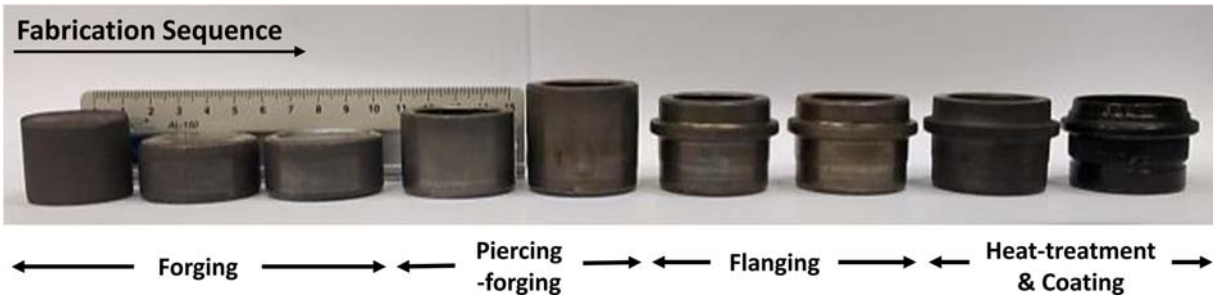

Fig. 2. Low-magnification photographs showing fabrication processes of an actual component of a cold heading quality steel wire rod of the 4C steel, which are composed of several hits such as forging, piercing-forging, and flanging.

nent of a cold-heading-quality steel wire rod of the 4C steel, which are composed of several hits such as forging, piercing-forging, and flanging. In order to simulate these processes, the split Hopkinson's pressure bar aforementioned in the section 2.3 was used. Cylindrical specimens (diameter; 4 mm, height; 8 mm) were prepared to be dynamically compressed by several hits of a striker bar. The specimen situated between incident and transmitter bars was compressed five times by a striker bar projected at a high speed using an air pressure of 0.05 MPa, 0.05 MPa, 0.1 MPa, 0.1 MPa, and 0.15 MPa in consideration of progressive strain hardening effect of the specimen and sufficient compressive deformation at each hitting step. The compressively deformed specimen was collected at each hitting step to examine the deformed microstructure and hardness.

3. RESULT

3.1. Microstructure

Figures 3(a) through (d) show optical micrographs of the four steel wire rods. The 2C, 3C, and 4C steels consist of ferrite and pearlite. Band structures of ferrite and pearlite are well developed inside rods. The volume fractions of pearlite are 27, 44, 66, and 100 % for the 2C, 3C, 4C, and 8C steels, respectively, and are roughly matched with those obtained from a lever rule in plain carbon steels [20]. The 8C steel has a full pearlitic microstructure, although the C content is slightly deviated from the typical eutectoid composition by a small addition of Mn, Si, and Cr (Table 1).

3.2. Dynamic compressive properties

Dynamic compressive stress-strain curves of the four steels are shown in Fig. 4, and their yield compressive strength, maximum compressive strength, and plastic strain are summarized in Table 2. In the curves, the early flow stress for the ductile metal cannot be accurate because it takes a finite amount of time for the strain rate to increase from zero to a desired level [19]. In the present study, thus, the yield strength is determined to be the strength at the strain of 0.5%. It can be expected that the impact of striker bar is transferred to the

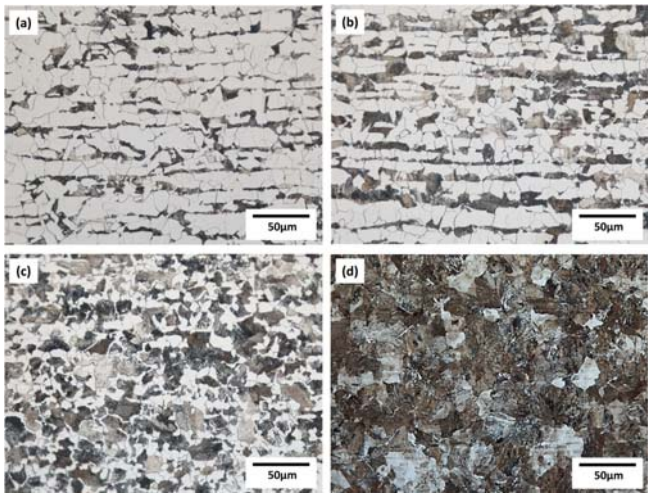

Fig. 3. Optical micrographs of the (a) 2C, (b) 3C, (c) 4C, and (d) 8C steels. The 2C, 3C, and 4C steels consist of ferrite and pearlite, whereas the 8C steel has a full pearlitic microstructure.

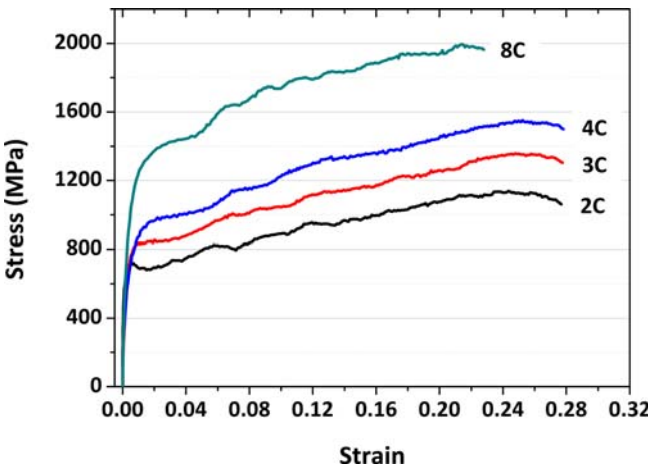

Fig. 4. Dynamic compressive stress-strain curves of the four steels. The dynamic compressive stress increases with increasing strain as the impact energy is continuously absorbed into the specimen.

one-dimensional compressive elastic energy, as one-dimensional elastic wave is generated along a long incident bar [18,19]. The dynamic compressive stress increases with increasing

Table 2. Room-temperature dynamic compressive test results of the four steels

Steel	Yield Strength (MPa)	Maximum Strength (MPa)	Plastic Strain (%)
2C	691 ± 25	1165 ± 37	27.7
3C	765 ± 45	1325 ± 46	28.2
4C	941 ± 16	1553 ± 3	27.9
8C	1362 ± 61	2018 ± 32	23.6

strain as the impact energy is continuously absorbed into the specimen. The 2C steel has the yield strength, maximum strength, and plastic strain of 691 MPa, 1165 MPa, and 27%, respectively. With increasing C content, the yield and maximum strengths increase, while the plastic strain remains almost constant. Since all the dynamic compressive specimens are not fractured, the plastic strain does not mean the fracture strain, but is the strain amount deformed by the one-time hit of the striker bar [19]. Thus, the strongest 8C steel shows the lowest plastic strain.

3.3. Cold-forging simulation results

Five-time forging simulation tests were performed by using a split Hopkinson's pressure bar, and the test results are summarized in Fig. 5 and Table 3. At each hitting step, the specimen height was measured and then normalized (divided by the original specimen height (8 mm)). In the 2C steel, the normalized height is 0.9 after the first hit, and continuously decreases after the subsequent hits. In the 8C steel, the normalized height is higher (0.95) than the 2C steel, which means that the deformation is more difficult in the 8C steel. The normalized height decreases continuously in all the steels as the number of hits increases.

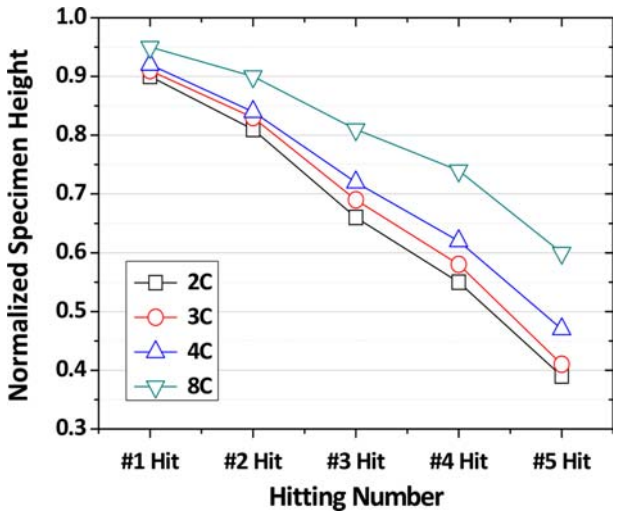

Fig. 5. Normalized specimen height measured from the five-time forging simulation test of the four steels. The normalized height continuously decreases after the subsequent hits.

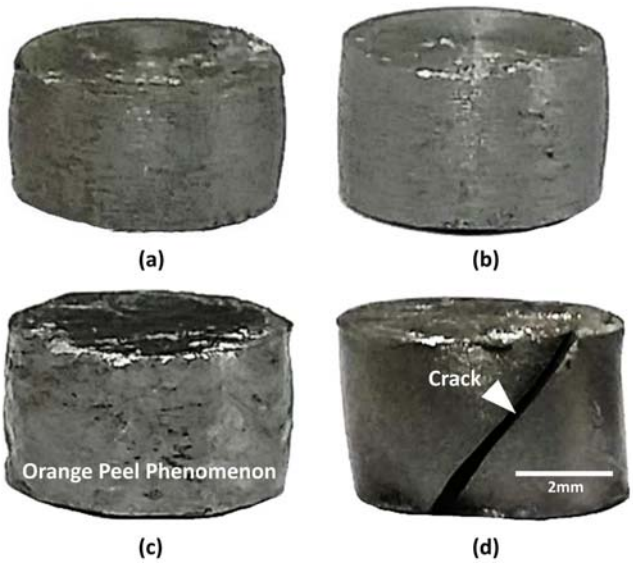

Fig. 6. Low-magnification optical photographs showing overall forging-simulated specimen shapes deformed after the fifth hit of the (a) 2C, (b) 3C, (c) 4C, and (d) 8C steels.

Figures 6(a) through (d) are low-magnification optical photographs showing overall forging-simulated specimen shapes deformed after the fifth hit. The 2C and 3C steels maintain the smooth specimen surface (Figs. 6(a) and (b)), but the 4C steel shows an orange peel effect on its rough specimen surface (Fig. 6(c)) [19]. In the 8C steel, a deep crack is formed along the 45° direction, although it is not completely separated (Fig. 6(d)).

The forging-simulated specimens in Figs. 6(a) through (d) were cross-sectioned in parallel along the compressive direction, and their low-magnification optical micrographs are shown in Figs 7(a) through (d). Localized shear deformation zones are formed diagonally inside dynamically compressed specimens, as indicated by dotted rectangles in Figs. 7(a) through (d), and develop into adiabatic shear bands [12]. In the 8C steel, the shear band appears to be white-colored and very narrow (Fig. 7(d)), which implies a different characteristic

Table 3. Normalized specimen height measured from the five-time forging simulation test of the four steels

Steel	#1 Hit (0.05 MPa)	#2 Hit (0.05 MPa)	#3 Hit (0.1 MPa)	#4 Hit (0.1 MPa)	#5 Hit (0.15 MPa)
2C	0.90	0.81	0.66	0.55	0.39
3C	0.91	0.83	0.69	0.58	0.41
4C	0.92	0.84	0.72	0.62	0.47
8C	0.95	0.90	0.81	0.74	0.60

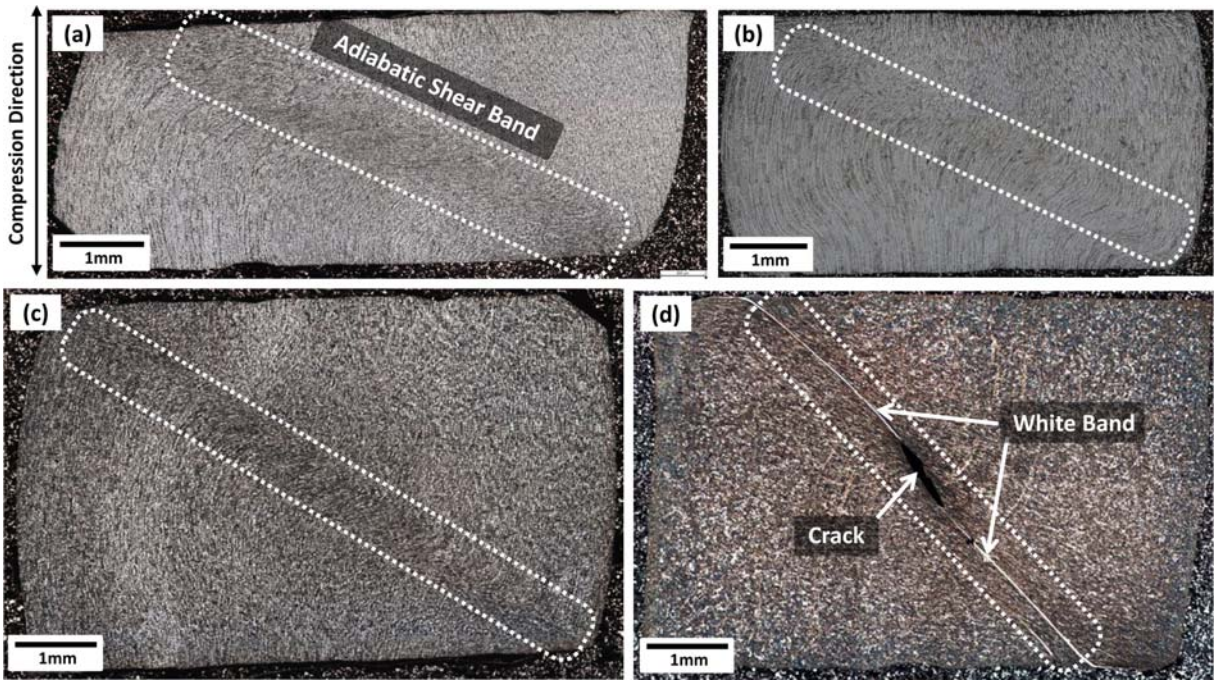

Fig. 7. Low-magnification optical micrographs of the cross-sectioned areas of the forging-simulated specimens after the fifth hit of the (a) 2C, (b) 3C, (c) 4C, and (d) 8C steels. Localized shear deformation zones are formed diagonally inside dynamically compressed specimens.

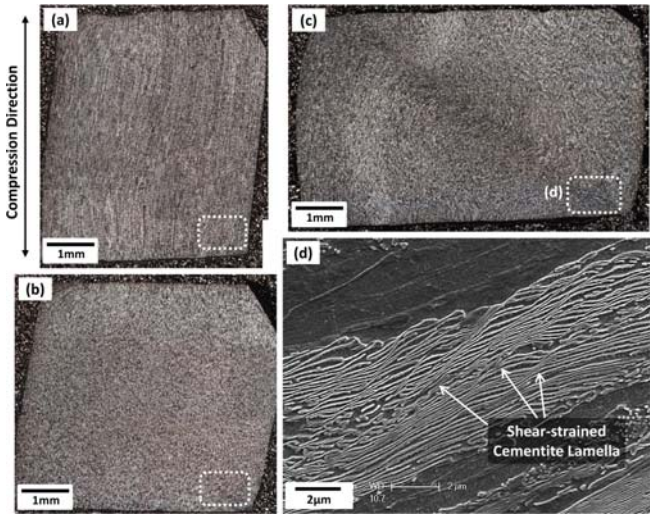

Fig. 8. Optical micrographs of the cross-sectioned areas of the forging-simulated specimens after the (a) third, (b) fourth, and (c) fifth hit of the 4C steel. (d) is a magnified SEM micrograph of a dotted rectangle in (c).

from other shear bands formed in the 2C, 3C, and 4C steels [12,21]. This shear band is more clearly visible than the other bands, and a long crack is formed along it, as indicated by an arrow in Fig. 7(d). The crack might propagate into the surface area to form the deep crack in Fig. 6(d).

Figures 8(a) through (c) show adiabatic shear band formation processes developed by the hitting steps in the 4C steel. An adiabatic shear band is weakly formed in an edge after the third hit as indicated by a dotted rectangle in Fig. 8(a). The shear strain of this band is measured to be approximately 30%. After the fourth hit, an adiabatic shear band is more clearly observed (Fig. 8(b)), and its shear strain increases to 220%. After the fifth hit, two diagonal edges are connected by a long adiabatic shear band whose width and shear strain are about 560 μm and 670 %, respectively (Fig. 8(c)). Within this shear band, ferrite and pearlite grains are extremely elongated. Fig. 8(d) is a magnified SEM micrograph of a dotted rectangle in Fig. 8(c). Cementite lamellas are sheared in a parallel mode inside a pearlite grain as the pearlite is heavily shear-strained, as indicated by arrows in Fig. 8(d). The widths and shear strains of adiabatic shear bands formed in the four steels were measured after the third, fourth, and fifth hits, and are summarized in Table 4. As the carbon content or the number of hit increases, the width of adiabatic shear band decreases, while its shear strain increases.

Table 4. Width and shear strain of adiabatic shear band measured after the third, fourth, and fifth hits in the forging simulation test

Steel	Width (μm)	Shear Strain (%)		
	#5 Hit	#3 Hit	#4 Hit	#5 Hit
2C	970	10*	150*	310
3C	630	40*	240*	420
4C	560	33*	220*	670
8C	50	-	-	Very High**

*The adiabatic shear band is not completely formed.
**The shear strain inside white-colored and very narrow band is very high (above 1000%).

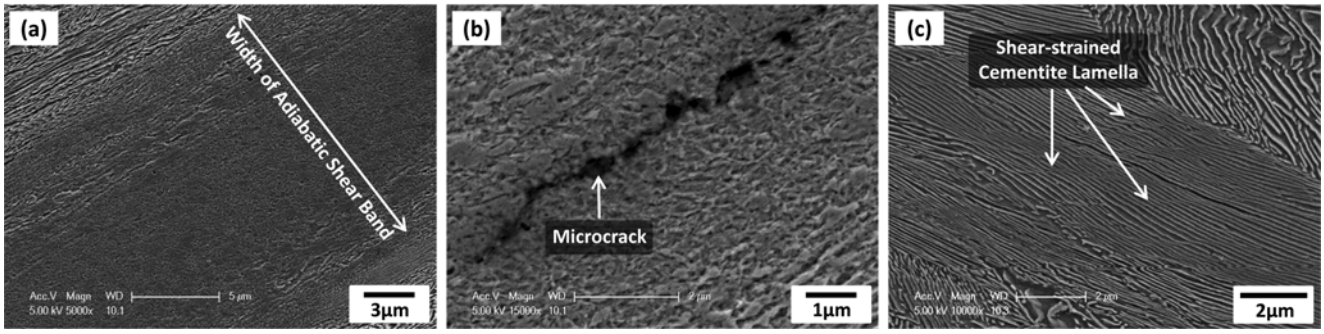

Fig. 9. (a) and (b) SEM micrographs of an adiabatic shear band formed after the fifth hit of the 8C steels. (c) is an SEM micrograph showing a number of cementite lamellas sheared in a parallel mode after the fourth hit of the spheroidized 8C steel.

Table 5. The Vickers hardness data of the forging-simulated specimens of the four steels. (unit: VHN)

Steel	As-Received	#1 Hit (0.05 MPa)	#2 Hit (0.05 MPa)	#3 Hit (0.1 MPa)	#4 Hit (0.1 MPa)	#5 Hit (0.15 MPa)
2C	145	167	176	206	210	235
3C	175	193	215	237	243	274
4C	198	246	262	267	279	279
8C	332	359	404	423	423	431

Figures 9(a) and (b) are SEM micrographs of an adiabatic shear band formed after the fifth hit of the 8C steel. The interior microstructure of shear band in the 8C steel is quite different from those of other steels because it shows a white band characteristic (Fig. 7(d)). It is composed of ultrafine grains whose size is smaller than 1 μm, whereas pearlite grains are heavily elongated outside the band (Fig. 9(a)). It also contains some microcracks as shown in high-magnification SEM micrograph (Fig. 9(b)). In order to investigate the adiabatic shear banding process of the 8C steel, an adiabatic shear band formed after the fourth hit is observed as shown in Fig. 9(c). A white band characteristic does not appear, but a number of cementite lamellas sheared in a parallel mode are found without forming microcracks or ultrafine grains.

The hardness in the center region of the forging-simulated specimen was measured at each hitting step, and the results are shown in Table 5. The hardness increases with increasing C content before the simulation test, which reflects the volume fraction of pearlite. In all the steels, the hardness continuously increases as the hitting number and C content increase, but its increased extent tends to be larger in the low-carbon steels than in the high-carbon steels.

4. DISCUSSION

4.1. Development of adiabatic shear band

In order to prevent the cracking phenomenon occurring during cold forging of cold-heading-quality steel wire rods, it is essential to improve metal flow and to reduce the formation of adiabatic shear bands. However, plain carbon steels are vulnerable to the adiabatic shear banding and cracking due to shearing of pearlite. In this study, the adiabatic shear banding phenomena are analyzed, and shear deformation characteristics are examined by the cold-forging simulation test using the dynamic compressive test to experimentally evaluate the extent of the adiabatic shear banding.

Adiabatic shear bands are readily formed as strain rate increases because of thermo-mechanical instability [22-25]. Plain carbon steels show homogeneous deformation with a relatively wide shear band region under quasi-static loading [26], whereas they tend to have localized deformation with a narrowed shear band region under dynamic loading. The dynamic process of adiabatic shear banding can roughly be divided into following three stages [8,16,27]: (1) homogeneous deformation stage, (2) inhomogeneous deformation stage, and (3) initiation and propagation stage of an adiabatic shear band due to localization of shear strain. This final stage is accompanied by the abrupt local temperature rise and the rapid reduction of shear stress. Such a localized deformation deteriorates the load carrying capability.

Considering the adiabatic shear band formation by thermo-mechanical instability arising from plastic instability and local temperature rise, a certain starting point of the shear banding exists as hitting steps are continuously proceeded during the cold-forging simulation test. In the present plain carbon steels, shear bands are formed in specific regions where plastic flow is concentrated, *e.g.*, regions diagonally connected between edges, after the fifth hit (Figs. 7(a) through (d)), whereas they are weakly formed at edges after the third or fourth hit (Figs. 8(a) and (b)). In particular, after the fifth hit of the 8C steel, the shear deformation is heavily localized along the diagonal region (Fig. 7(d)), thereby leading to the cracking under the same forging simulation condition (Fig.

6(d)). These results imply that the adiabatic shear banding proceeds step by step during the cold-forging simulation test as the number of hit increases.

Besides thermo-mechanical instability factors, microstructural factors also significantly affect the cold forging. Since the readiness of the shear band formation varies with the microstructural change [8,28-30], the microstructure should precisely be analyzed throughout the processes of adiabatic shear banding. Main microstructural factors of the present plain carbon steels are grain size and volume fraction and shape of pearlite. Pearlites deteriorate the plastic flow because they can be heavily shear-strained and facilitate themselves as microcracking or shear-cracking sites [14,31]. For example, cementite lamellas of pearlite grains are sheared in a parallel mode as they are critically shear-strained after the fourth or fifth hit (Figs. 8(d) and 9(c)). Considering this negative effect of pearlite, it can be expected that the higher its volume fraction is, the easier is the adiabatic shear banding. Thus, adiabatic shear bands are heavily formed in the order of the 2C, 3C, 4C, and 8C steels as the volume fraction of pearlite increases, which is well matched with the adiabatic shear banding data in Table 4.

It is interesting to note from Fig. 7(d) that a very narrow white-colored shear band is formed in the 8C steel. According to previous researches on adiabatic shear bands [12,21,32-34], this white band can be classified into a transformed shear band, instead of a locally deformed shear band, because the phase transformation occurs by the temperature rise up to the austenite region [12,21]. However, there is no clear evidence to prove that the material within the band underwent the phase transformation. Beatty *et al*. [35] reported that the white band was probably related with grain refinement caused by severe deformation. According to Timothy [36], the transformed band might correspond to an advanced stage of adiabatic strain localization as it was closely related with the locally deformed band representing an earlier stage of adiabatic shear banding. In the present 8C steel, the localized deformation region is observed at pearlite grains in the early stage of adiabatic shear banding (Fig. 9(c)), and it develops to the white band after the one more hitting step (Figs. 7(d) and 9(a)). Thus, the white band formed in the 8C steel would be a transformed band, although the temperature rise within the band is not measured or estimated in this study.

4.2. Interpretation of adiabatic shear banding or cracking by cold-forging simulation tests

Forgery producers have been increasingly using precision forging in which complicated parts can be formed directly in near-net-shape or net-shape in order to achieve the durability and quality as well as cost reduction. Particularly in cold forging of plain carbon steels, steels generally require the high formability which can accommodate severe deformation. However, cracks are often formed at edges of parts where the deformation is highly concentrated. In the present study, the 2C and 3C steels are dynamically compressed without surface defects after the fifth hit, but an orange peel phenomenon is observed on the surface of the 4C steel. This orange peel phenomenon is one of typical surface defects, and is hardly found in steels having sufficiently high formability. This implies that the further deformation is not allowable after the fifth hit of the 4C steel, and that the orange peel phenomenon might induce the surface cracking [37].

The formation of adiabatic shear band is closely related with the cracking during the forging process [21,32]. In the 8C steel, a deep crack is formed along the 45° direction after the fifth hit (Fig. 6(d)), and a strong adiabatic shear band is found (Fig. 7(d)), along which a crack is formed. In order to prevent the cracking of the 8C steel, the spheroidization treatment is essentially required. Thus, the 8C steel was commercially spheroidization-treated at 750 °C (right above the A_1 temperature) for 6 hrs followed by holding at 710 °C (right below the A_1 temperature) for 15 hrs. Figure 10(a) is a low-magnification optical micrograph showing the forging-simulated specimen deformed after the fifth hit of the spheroidized 8C steel. Inhomogeneously deformed regions are observed along the diagonal direction of the specimen, but do not develop into an adiabatic shear band. SEM micrographs of the scarcely deformed and inhomogeneously deformed regions, as marked by blue and white dotted rectangles in Fig. 10(a), are shown in Figs 10(b) and (c), respectively. Lamellar cementites inside pearlite grains are well spheroidized after the spheroidization, and spheroidal cementites are homogeneously distributed in the ferrite matrix (Fig. 10(b)). Spheroidal cementites are maintained in the inhomogeneously deformed region (Fig. 10(c)), while the ferrite matrix is slightly deformed (Fig. 10(d)). In the spheroidized 8C steel, thus, adiabatic shear bands or cracks are not found at all during the forging simulation test as the specimen is mostly homogeneously deformed. This indicates that the spheroidization treatment can effectively prevent the adiabatic shear banding or cracking occurring during the forging process.

In this study, microstructures and dynamic compressive characteristics of four plain carbon steels are analyzed in relation with the intensity of the adiabatic shear banding and cracking. Based on the analyses, suggestions are made to forecast the cracking as well as to prevent it during cold forging. Since studies on dynamic compressive characteristics, besides the adiabatic shear banding, provide excellent data in evaluating the cold-forging performance, further researches should be made on alloy design and microstructural and process parameters in order to prevent the cracking. In addition, the spheroidization treatment, which is compulsorily used prior to the cold forging for preventing the cracking, should be carefully considered because it cannot be useful for low-carbon steels such as the present 2C, 3C, and 4C steels or for moderate

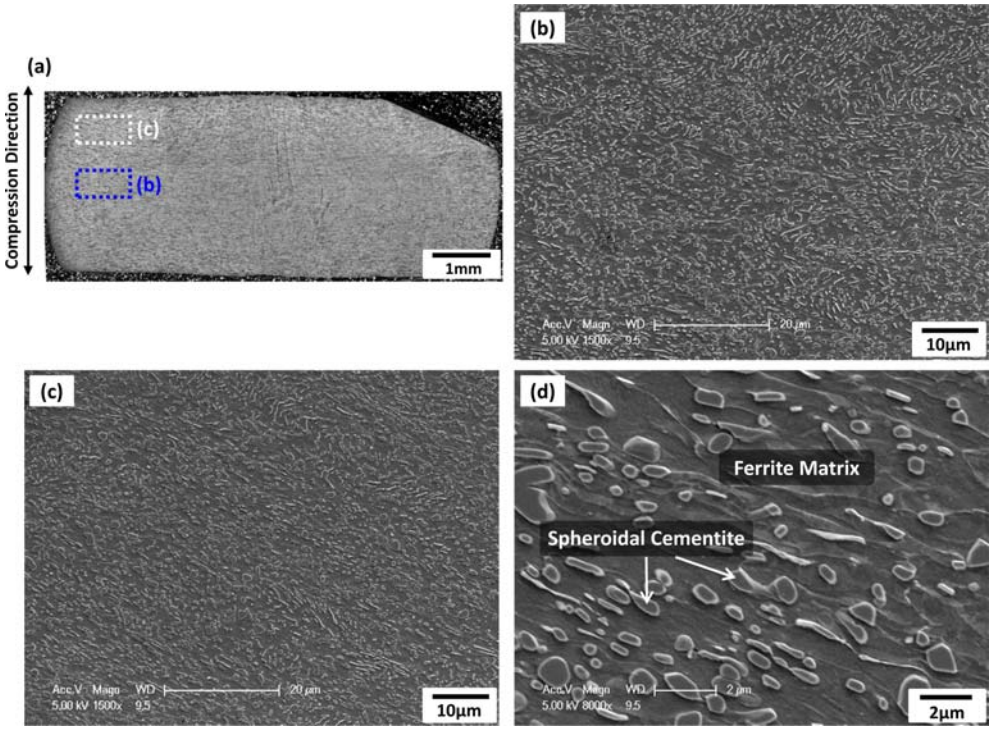

Fig. 10. (a) Optical and (b) through (d) SEM micrographs showing the forging-simulated specimen deformed after the fifth hit of the spheroidized 8C steel. (b) and (c) are SEM micrographs of the scarcely deformed and inhomogeneously deformed regions, as marked by blue and white dotted rectangles in (a), respectively.

forging conditions. The present cold-forging simulation test effectively evaluates the cold-forging performance by controlling the air pressure simulating the number and amount of hit, and provides an important idea on whether the spheroidization is needed or not.

5. CONCLUSIONS

In the present study, microstructures and dynamic compressive properties of plain carbon steels, whose carbon content was varied from 0.2 to 0.8 wt%, were investigated in relation with intensity of adiabatic shear banding, and cracking possibilities during cold forging were analyzed by a cold-forging simulation test using a split Hopkinson's pressure bar.

(1) The 0.2C, 0.3C, and 0.4C steels consisted of ferrite and pearlite in a band structure, and the 0.8C steel had a full pearlitic microstructure. The dynamic compressive test results indicated that the dynamic compressive stress increased with increasing strain as the impact energy was continuously absorbed into the specimen. With increasing C content, the yield and maximum strengths increased, while the plastic strain remained almost constant. Since all the dynamic compressive specimens were not fractured, the plastic strain did not mean the fracture strain, but was the strain amount deformed by the one-time hit of the striker bar. Thus, the strongest 0.8C steel showed the lowest plastic strain.

(2) Five-time forging simulation tests were performed by using a split Hopkinson's pressure bar. The 0.2C and 0.3C steels were dynamically compressed without surface defects after the fifth hit, but an orange peel phenomenon was observed on the surface of the 0.4C steel. This implied that the further deformation was not allowable after the fifth hit of the 0.4C steel, and that the orange peel phenomenon might induce the surface cracking. In the 0.8C steel, a deep crack was formed along the 45° direction, although it was not completely separated.

(3) In all the steels, the localized shear deformation zones were formed diagonally inside dynamically compressed specimens, and were developed into adiabatic shear bands. Within shear bands, ferrite and pearlite grains were extremely elongated, and cementite lamellas were sheared in a parallel mode. The higher the volume fraction of pearlite was, the easier was the adiabatic shear banding, and thus adiabatic shear bands were heavily formed in the order of the 0.2C, 0.3C, 0.4C, and 0.8C steels. Particularly in the 0.8C steel, the shear band appeared to be white-colored and very narrow, along which a long crack was formed. This transformed shear band was composed of ultrafine grains whose size was smaller than 1 μm, whereas pearlite grains were heavily elongated outside the band.

(4) In order to prevent the cracking of the 0.8C steel, the

spheroidization treatment was essentially required. In the spheroidized 0.8C steel, adiabatic shear bands or cracks were not found at all during the forging simulation test as the steel was relatively homogeneously deformed. This indicated that the spheroidization effectively prevented the adiabatic shear banding or cracking occurring during the forging process. The present forging simulation test plausibly evaluated the cold-forging performance by controlling the number and amount of hit, and provided an important idea on whether the spheroidization was needed or not.

ACKNOWLEDGMENTS

This work was supported by POSCO under a contract No. 2012Y023, and by Brain Korea 21 PLUS Project for Center for Creative Industrial Materials.

REFERENCES

1. A. Iwama and I. Nomura, *U. S. Patent 5*, **362**, 338 (1994).
2. H. Kim, M. Kang, C. M. Bae, H. S. Kim, and S. Lee, *Metall. Mater. Trans. A* **45A**, 1294 (2014).
3. K.-H. Kim, S.-D. Park, J.-H. Kim, and C.-M. Bae, *Met. Mater. Int.* **18**, 917 (2012).
4. B. Hwang, T.-H. Lee, J.-H. Shin, and J.-W. Lee, *Korean J. Met. Mater.* **52**, 21 (2014).
5. A. Marchand and J. Duffy, *J. Mech. Phys. Solids* **36**, 251 (1988).
6. S. N. Medyanik, W. K. Liu, and S. Li, *J. Mech. Phys. Solids* **55**, 1439 (2007).
7. R. G. O'Donnell and R. L. Woodward, *J. Mater. Sci.* **23**, 3578 (1988).
8. D.-K Kim, S. Y. Kang, S. Lee, and K. J. Lee, *Metall. Mater. Trans. A* **30A**, 81 (1999).
9. H. L. Park, K. C. Jin, S. J. Baek, and C. S. Choi, *J. Kor. Inst. Met. Mater.* **29**, 220 (1991)
10. K. Cho, Y. C. Chi, and J. Duffy, *Metall. Trans. A* **21A**, 1161 (1990).
11. P. R. Guduru, A. J. Rosakis, and G. Ravichandran, *Mech. Mater.* **33**, 371 (2001).
12. Y. Bai and B. Dodd, *Adiabatic Shear Localization-Occurrence, Theories, and Applications*, p.10, Pregamon Press, New York (1992).
13. J. L. Sun, P. W. Trimby, F. K. Yan, X. Z. Liao, N. R. Tao, and J. T. Wang, *Acta Mater.* **79**, 47 (2014).
14. A. Sabih and J. A. Nemes, *J. Mater. Process. Tech.* **209**, 4292 (2009).
15. M. S. Salehi, N. Anjabin, and H. S. Kim, *Met. Mater. Int.* **20**, 825 (2014).
16. K. Cho, S. Lee, J. Duffy, and S. R. Nutt, *Acta Metall.* **41**, 923 (1993).
17. H. S. Kim, S.-H. Joo, and H. J. Jeong, *Korean J. Met. Mater.* **52**, 87 (2014).
18. E. D. H. Davies and S. C. Hunter, *J. Mech. Phys. Solids* **11**, 155 (1963).
19. W. Chen and B. Song, *Split Hopkinson (Kolsky) Bar-Design, Testing, and Applications*, p.7, Springer, New York (2011).
20. R. C. Creese, *Introduction to Manufacturing Processes and Materials*, pp.36-37, Marcel Dekker, Inc., New York (1999)
21. B. Dodd and Y. Bai, *Adiabatic Shear Localization-Frontiers and Advances*, pp.111-171, Elsevier, Amsterdam (2012).
22. T. Weerasooriya and J. Clayton, *Proc. 2006 Int. Conf. on Tungsten, Refractory & Hardmetals VI*, pp.1-9, Metal Powder Industries Federation, Orlando, Florida (2006).
23. Z. Xiaoqing, L. Shukui, L. Jinxu, W. Yingchun, and W. Xing, *Mater. Sci. Eng. A* **527**, 4881 (2010).
24. G. R. Johnson and J. M. Hoegfeldt, U. S. Lindholm, A. Nagy, *Trans. ASME* **105**, 42 (1983).
25. Y. P. Song, W. K. Wang, D. S. Gao, E. Y. Yoon, D. J. Lee, and H. S. Kim, *Met. Mater. Int.* **20**, 445 (2014).
26. C. L. Wittman, M. A. Meyers, and H.-R. Pak, *Metall. Trans. A* **21A**, 707 (1990).
27. S. Lee, K.-M. Cho, K. C. Kim, and W. B. Choi, *Metall. Trans. A* **24A**, 895 (1993).
28. K. T. Ramesh and R. S. Coates, *Metall. Trans. A* **23A**, 2625 (1992).
29. R. L. Woodward, N. J. Baldwin, I. Burch, and B. J. Baxter, *Metall. Trans. A* **16A**, 2031 (1985).
30. J. Lankford, A. Bose, and H. Couque, *High Strain rate Behavior of Refractory Metals and Alloys* (eds. R. Asfahani, E. Chen, and A. Crowson), p.267, TMS, Cincinnati, OH (1992).
31. R. W. K. Honeycombe, *Steels-Microstructure and Properties*, Third ed., p.63, Edward Arnold, London (2006).
32. S. Boakye-Yiadom and M. N. Bassim, *Mater. Sci. Eng. A* **528**, 8700 (2011).
33. L. Tang, Z. Chen, C. Zhan, X. Yang, C. Liu, and H. Cai, *Mater. Charact.* **64**, 21 (2012).
34. Y. Xu, J. H. Zhang, Y. L. Bai, and M. A. Mayers, *Metall. Mater. Trans. A* **39A**, 811 (2008).
35. J. H. Beatty, L. W. Meyer, M. A. Meyers, and S. Nemat-Nasser, *Shock-Wave and High-Strain-Rate Phenomena* (eds. M. A Meyers, L. E. Murr, K. P. Staudhammer), pp.645-656, Marcel Dekker, NewYork (1992).
36. S. P. Timothy, *Acta Metall.* **35**, 301 (1987).
37. H.-S. Kim and Y.-T. Im, *Trans. ASME* **121**, 336 (1999).